Influence of post-treatment time of trivalent chromium protection coating on aluminium alloy 2024-T3 on improved corrosion resistance

Anca-Iulia Stoica, Jolanta Świątowska, Alexandre Romaine, Francesco Di Franco, Jiantao Qi, Dimitri Mercier, Antoine Seyeux, Sandrine Zanna, Philippe Marcus

Influence of post-treatment time of trivalent chromium protection coating on aluminium alloy 2024-T3 on improved corrosion resistance

Article *in* Surface and Coatings Technology · April 2019

DOI: 10.1016/j.surfcoat.2019.04.051

9 authors, including:

Anca-Iulia Stoica

52 PUBLICATIONS **409** CITATIONS

SEE PROFILE

Jolanta Światowska

French National Centre for Scientific Research

73 PUBLICATIONS **1,516** CITATIONS

SEE PROFILE

Alexandre Romaine

Vallourec

11 PUBLICATIONS **66** CITATIONS

SEE PROFILE

Francesco Di Franco

Università degli Studi di Palermo

43 PUBLICATIONS **280** CITATIONS

SEE PROFILE

Influence of post-treatment time of trivalent chromium protection coating on aluminium alloy 2024-T3 on improved corrosion resistance

Anca-Iulia Stoica, Jolanta Światowska, Alexandre Romaine, Francesco Di Franco, Jiantao Qi, Dimitri Mercier, Antoine Seyeux, Sandrine Zanna, Philippe Marcus

PII: S0257-8972(19)30422-0
DOI: https://doi.org/10.1016/j.surfcoat.2019.04.051
Reference: SCT 24546

To appear in: *Surface & Coatings Technology*

Received date: 14 December 2018
Revised date: 14 March 2019
Accepted date: 13 April 2019

Please cite this article as: A.-I. Stoica, J. Światowska, A. Romaine, et al., Influence of post-treatment time of trivalent chromium protection coating on aluminium alloy 2024-T3 on improved corrosion resistance, Surface & Coatings Technology, https://doi.org/10.1016/j.surfcoat.2019.04.051

Influence of post-treatment time of Trivalent Chromium Protection coating on Aluminium Alloy 2024-T3 on improved corrosion resistance

Anca-Iulia Stoica[a,1], Jolanta Świątowska[a*], Alexandre Romaine[a,2], Francesco Di Franco[a,3], Jiantao Qi[a,4], Dimitri Mercier[a], Antoine Seyeux[a], Sandrine Zanna[a] and Philippe Marcus[a*]

[a]PSL Research University, Chimie ParisTech – CNRS, Institut de Recherche de Chimie Paris, 11 rue Pierre et Marie Curie, 75005 Paris, France

Abstract

Low corrosion protection performances of Trivalent Chromium Process (TCP) coatings with reference to Chromium Conversion Coatings (CCC) deposited on aluminium alloys can be overcome by application of post-treatment processes. This work shows the effect of post-treatment bath (containing hydrogen peroxide and lanthanum salt) on the chemical composition, structure and the corrosion performances of TCP coating deposited on AA 2024-T3 aluminium alloy. Different times of post-treatment bath were applied on the TCP coating and the samples were analyzed by Time-of-Flight Secondary Ion Mass Spectrometry (ToF-SIMS), X-ray Photoelectron Spectroscopy (XPS) and Glow Discharge -Optical Emission Spectrometry (GD-OES). The ToF-SIMS and GD-OES depth profiles show that the post-treatment time has no influence on the thickness of the TCP coating and on its bi-layered structure. It is composed of an outer layer, rich in zirconium and chromium oxides and an inner layer rich in aluminium oxides and oxy-fluorides. 3D ToF-SIMS images reveal an enrichment of Cr and Zr-like species over the surface of intermetallic particles with reference to alloy matrix, whereas a homogenous distribution of La is observed. The analysis of in-depth distribution shows that La is present principally in the outer part of the TCP coating. The La concentration increases with increasing post-treatment time. The effect of post-treatment time on protection was evaluated by Electrochemical Impedance Spectroscopy (EIS) and Linear Sweep Voltammetry (LSV) in a 0.001 M NaCl + 0.1 M Na_2SO_4 electrolyte. The increased post-treatment time enhances the cathodic inhibition against oxygen reduction. The post-treatment provides improved coating homogeneity and sealing properties.

Keywords: trivalent chromium protection coating; post-treatment; corrosion; ToF-SIMS; XPS; GD-OES

1. Introduction

* Corresponding authors:
Jolanta Świątowska, email: jolanta.swiatowska@chimieparistech.psl.eu, tel: +33(0)144278026,
Philippe Marcus, email: philippe.marcus@chimieparistech.psl.eu, tel: +33(0)144272638

Present addresses:
[1] Pro Aqua Diamantelektroden Produktion GmbH, A-8712 Niklasdorf, Parkring 1, Austria
[2] Vallourec Research Center France, 60 route de Leval, F-59620 Aulnoye-Aymeries, France
[3] Dipartimento di Ingegneria Civile, Ambientale, Aerospaziale e dei Materiali (DICAM), Università degli Studi di Palermo, Viale delle Scienze, Edificio 6, 90128 Palermo, Italy
[4] College of Chemical Engineering, China University of Petroleum (East China), Qingdao, 266580, P. R. China

Aluminium alloy 2024 is widely used in aircraft industries due to its excellent mechanical properties, light mass, high strength and damage tolerance [1]. However, it has been shown that this aluminium alloy is susceptible to localized corrosion, especially due to the heterogeneous distribution of copper in the alloy, with copper-rich intermetallic particles [2]. The role of intermetallic particles for the initiation and propagation of localized corrosion on the aluminium alloys is well-known [3,4]. For 2024-T3 aluminium alloy, Al_2CuMg, Al_2Cu and Al_6(Cu, Fe, Mn) are the main three intermetallic inclusions. It was reported that Al_2CuMg acted as an active phase and Al_2Cu and Al_6(Cu, Fe,Mn) acted as noble phases [4,5]. It was also found that the dealloying of Mg and Al simultaneously happened on Al_2CuMg particles at the initial stage of corrosion process. At the same time, the corrosion of Al matrix surrounding the particles occurred [6]. Two main types of localized corrosion occur on AA 2024 in the neutral chloride solutions, namely, pitting corrosion and corrosion along the grain boundaries. Thus, effective inhibitors and coatings are necessary to suppress the dealloying of Al_2CuMg and also protect the Al matrix from localized corrosion [7,8].

Chromate conversion coatings (CCCs) have been applied for several decades, but due to the highly toxic hexavalent chromium present in the CCCs, its application is going to be restricted in Europe (REACh requirements) [9] and in the United States [10]. The application of CCCs will be banned by 2024 by the European Community. Thus, different solutions have been developed for replacing CCCs. Recent researches have been focused on Cr(VI)-free conversion coatings, with low pollution effect, low toxicity, and harmless to human beings. Conversion coatings prepared in non-Cr(VI) containing solutions, such as titanium, zirconium, molybdenum, cerium, and trivalent chromium, have been extensively studied [6,11-13]. In the last decade all the studies concerning corrosion protection of aluminium alloys were based on green treatments and one of the promising alternatives for chromates was Trivalent Chromium Process (TCP), or Trivalent Chromium Conversion (TCC) coatings (containing ZrF_6^{2-}, Cr^{3+}, SO_4^{2-} and F^- salts with a pH of 3.8–4.0), which have been shown to provide good corrosion protection and paint adhesion in standardized

tests according to ASTM D3359 methods [14-17]. The coating formation involves the dissolution of the native oxide on the aluminium surface due to the acidic, fluoride-containing solution, and the subsequent pH-driven deposition of zirconium and chromium species. On exposure to the TCP bath, a mixed oxide layer precipitates on the surface. The increase in interfacial pH is promoted by the cathodic reactions, i.e. hydrogen evolution and/or oxygen reduction [18-20].

It should be noted that TCP shows lower corrosion resistance performances than CCC [21]. Thus, to improve the corrosion performance of the TCP coatings a post-treatment can be applied. There is limited information in the literature about post-treatment of TCP conversion coatings, which lead to increased corrosion resistance of the conversion layers [22-25]. Qi *et al.* [22,26] studied the role of temperature and pH water immersion post-treatment on the coating microstructure and corrosion resistance and evidenced that immediate tap-water rinsing could offer reproducible structure and performance. The comparative studies revealed that the water immersion post-treatment at 40° C and pH 5 displayed the optimal coating performance. In contrast, the coating experienced a significant shrinkage in the alkaline water bath. With consideration of the presence of hydrated channels and defects in the TCC coatings, Li *et al.* [27] studied the effects of aging temperature and time on the physical structure and corrosion protection properties. They revealed that aging in air at room temperature from 1 to 7 days significantly enhanced by a four times the charge transfer resistance with negligible effect on coating thickness. In contrast, at temperature of 55 and 100 ^{o}C the coating thickness was reduced and the aging at 150 ^{o}C led to severe cracking and coating detachment from the substrate. Pearlstein *et al.* [16] first reported the performance of TCC coatings applied on aluminium alloys and employed peroxide as an oxidant to post-treat the coating surface. However, there is limited knowledge about such modified coating and its surface chemistry. In our previous studies [25], we have presented for the first time the role of the post-treatment bath based on peroxide and La (III) salts on the improved corrosion behavior of TCP coating. The influence of each bath component, peroxide and lanthanum salts, on the chemical composition and corrosion behavior of TCP coating was demonstrated. It is important to note that this post-treatment showed a

formation of small quantity of Cr(VI) (oxide/hydroxide) on the TCP coating surface not exceeding 0.1 wt% of the TCP coating. Considering the 1 mm thick aluminium alloy sheet coated by the post-treated TCP coating, it was calculated [25] that the maximum quantity of Cr(VI) could be around 4 $x10^{-5}$ wt%, which was concluded to be much lower than the 0.1 wt% of Cr (VI) authorized by REACh regulations [9]. Taking into account the promising corrosion properties of TCP post-treated coating further studies were conducted in our group.

In this work, we present the influence of post-treatment time in a bath based on hydrogen peroxide and lanthanum salts (Socosurf PACS) on the chemical composition, structure and the electrochemical performance of the TCP coated alloy. It was shown by the salt spray tests performed according to ASTM B117 standard that the application of Socosurf PACS post-treatment show the increased corrosion resistance to around 360 hours while around 96 hours are reached for the TCP samples without post-treatment [25]. The objective of this work was to better understand the post-treatment process on the TCP coating and to optimize the post-treatment process time. To do so, surface and coating/substrate interface properties were studied by X-ray Photoelectron Spectroscopy (XPS), Time-of-Flight Secondary Ion Mass Spectrometry (ToF-SIMS), Glow Discharge Optical Emission Spectrometry (GD-OES), combined with electrochemical characterization by Linear Sweep Voltammetry (LSV) and Electrochemical Impedance Spectroscopy (EIS).

2. Experimental procedures

Material, surface preparation and deposition of TCP layers and PACS post-treatment

AA 2024-T3 alloy samples with thickness of 3 mm with elemental composition of 0.5 % Si, 0.5 % Fe, 3.8-4.9 % Cu, 0.3-0.9 % Mn, 1.2-1.8 % Mg, 0.1 % Cr, 0.25 %Zn, 0.15 %Ti were used as substrate material. They were cut to a dimension of 8 mm × 8 mm.

The samples were mechanically grinded with 1200, 2400 grits paper, followed by polishing using 3,

1 and 0.3 µm alumina suspensions on a felt polishing pad. The samples were then successively sonicated in isopropanol, ethanol and ultrapure water (resistivity 18 MΩ·cm) for 2 minutes, respectively. Polishing was performed until the surface exhibited a mirror-like finish with no visible polishing striations. After that, the panels were dried by a compressed air stream at room temperature.

The fresh polished samples were degreased in a commercial solution (pH ≈ 9), composed of Sodium Tripolyphosphate, Borax, Turco 4215 additive at 60 ± 5 °C for 20 minutes. The degreased samples were rinsed in ultrapure water for 2 minutes and then immersed in deoxidizing solution, SOCOSURF A1858/A1806 (containing HNO_3, H_2SO_4 and Fe(III), pH ≤ 1) at 50°C for 5 minutes. The samples were then rinsed in ultrapure water for 2 minutes and immersed for 5 minutes in the SOCOSURF TCS (Trivalent Conversion and Sealing) solution denoted here as a Trivalent Conversion Process (TCP). The TCP treatment bath contained a mixture of Cr (III) and Zr (IV) salts. The bath pH, 3.8 < pH < 4.0, was monitored and adjusted before each use. The TCP coated samples were prepared by immersion in the TCP bath at 40°C for 10 minutes. For the post-treated samples, after TCP deposition, the samples were immersed in the post-treatment solution, SOCOSURF PACS (Passivation After Conversion and Sealing) composed of a mixture of La (III) salt and H_2O_2. The bath pH, 4.0 < pH < 5.0, was monitored and adjusted before each use. For the post-treatment conversion coating step, the samples were immersed in the PACS bath at 25°C for different times (5, 10, 30 minutes). The samples with or without post-treatments were rinsed in ultrapure water for 2 minutes, and then dried by compressed air at room temperature, followed by a 10 minutes drying in an oven at 60° C and ageing overnight at room temperature in a desiccator before surface and/or electrochemical characterization. The SOCOSURF TCS and SOCOSURF PACS [28] solutions are commercialized by Socomore (France) under a license of Mecaprotec (France).

Surface chemical characterization

The coated samples were analyzed by Time-of-Flight Secondary Ion Mass Spectroscopy (ToF-SIMS), Glow Discharge - Atomic Emission Spectrometry (GD-OES) and X-ray Photoelectron Spectroscopy (XPS).

A ToF-SIMS 5 spectrometer (IonToF) was used for in-depth profililing analyses. The spectrometer was run at an operating pressure of 10^{-9} mbar. A pulsed 25 keV Bi^+ primary ion source was employed for analysis, delivering 1.2 pA of current over a 100 × 100 μm^2 area. Negative ions depth profiling was performed by interlacing analysis with sputtering using a 2 keV Cs^+ sputter beam giving a 100 nA target current over a 400 × 400 μm^2 area. Positive ions depth profiling was performed by interlacing analysis with sputtering using a 2 keV O_2^+ sputter beam giving a 100 nA target current over a 300 × 300 μm^2 area. Data acquisition and post-processing data analysis were performed using the Ion-Spec commercial software version 4.1. A Veeco Dektak 150 contact profilometer was used to measure the depth of sputtered crater and to estimate the TCP layer thickness. The data were analyzed with the Dektak software.

A radio-frequency (rf) glow discharge optical emission spectrometer (GD-OES, GD-Profiler 2, HORIBA Scientific) was used for elemental depth profiles for TCP coated AA 2024-T3 samples without and with PACS post-treatment. Profiles have been carried out using a 4 mm-diameter anode. The discharge conditions were the following: pressure of 850 Pa and rf power of 50 W. The emission lines selected were 396.157 nm for Al, 339.203 nm for Zr, 425.439 nm for Cr, 625.00 nm for La. Before each profile, a plasma pre-treatment with silicon wafer was used to remove contaminants on the anode [29]. Good reproducibility of the data was checked by triple analyses for each specimen.

A VG ESCALAB 250 spectrometer was employed for XPS chemical characterization. The analysis chamber was at a pressure of∼ 10−9 mbar and Al Kα monochromatized radiation ($h\nu$ = 1486.6 eV) was used as the X-ray source. The spectrometer was calibrated against the reference binding energies (BE) of clean Cu (932.6 eV), Ag (368.2 eV) and Au (84 eV) samples. All analyses were performed at the take-off angle of 90◦. High resolution spectra (Al 2p, Cu 2p, Cr 2p, Zr 3d and La

5d) were collected with a pass energy of 20 eV. Peak fitting was performed with the Advantage software version 5.966 provided by Thermo Electron, using a Shirley-type background and Gaussian/Lorentzian peak shapes at a fixed ratio of 70/30. Binding energies of the component peaks were corrected with reference to the -CH-CH- binding energy of 285.0 eV.

Electrochemical measurements

All electrochemical measurements were performed in an air-saturated mixture of 0.1M Na_2SO_4 + 0.001M NaCl electrolyte at room temperature in a conventional, three-electrode cell. A saturated calomel electrode (SCE, E°=0.241 V *vs* SHE) was used as a reference electrode, a platinum as a counter electrode and a bare AA 2024-T3 sample after degreasing and deoxidation pre-treatment and a TCP-coated AA 2024-T3 sample without and with PACS post-treatment as a working electrode with an exposed area of 0.20 cm^2. An Autolab PGSTAT30 was used as a potentiostat/galvanostat. The Na_2SO_4 (Merck, Darmstadt, Germany) and NaCl (AnalR, NORMAPUR, VWR) solutions were prepared using the ultrapure water (resistivity 18 MΩ·cm).

The electrochemical measurements were started with measuring the open circuit potential (OCP) for 30 minutes, followed by the Electrochemical Impedance Spectroscopy (EIS) measurements in the frequency range from 10^{-2} to 10^{6} Hz in potentiostatic mode at the OCP and then followed by the Linear Sweep Voltammetry (LSV) from -1.1 to 0.6 V *vs* SCE with a scanning rate of 2 mV/s. The LSV scans were recorded at 2 mV/s. The EIS measurements were made using a 10 mV rms AC sine wave codded to the applied dc potential (OCP). To check the reproducibility, three samples were analyzed under the same conditions.

3. **Results and discussion**

3.1 Chemical composition and structure of PACS post-treated TCP layer

Figure 1 shows the ToF-SIMS negative ion depth profiles of TCP coating deposited on AA 2024-T3 substrate without (a) and with 5 minutes of PACS post-treatment (b) and positive ion depth profiles for the post-treated sample (c). The ion intensities are presented in logarithmic scale in order to emphasize the low intensity signals, and plotted versus Cs^+ sputtering time for negative ion depth profile and versus O^+ sputtering time for positive ion depth profiles. Negative ion depth profiles are used to study oxide species [30-33] and the positive ion depth profiles to study the metallic (lanthanum, zirconium and chromium) species [25].

In the case of the negative ion depth profiles presented for the TCP coating without and with PACS post-treatment presented in Figure 1 (a) and (b), respectively, the selected ions are $^{18}O^-$, AlO_2^-, Al_2^-, MgO^-, Cu^-, ZrO_2^-, CrO_2^-, $AlOF^-$. The comparison of these ion depth profiles was necessary in order to evaluate the influence of PACS bath on the stability of TCP layer. Three regions can be distinguished in these depth profiles, which are defined by intensity changes of ions corresponding to the TCP layer ($^{18}O^-$, ZrO_2^-, CrO_2^-, $AlOF^-$, AlO_2^-) and AA substrate (Al_2^-, MgO^-, Cu^-):

- the first one up to 150 s of sputtering time with a stable intensity of ZrO_2^-, and CrO_2^- ions is the outer TCP conversion coating region,
- the second one from around 150 to 310 s of sputtering, which is the coating/substrate interfacial region called also inner TCP with a decreasing intensity of ZrO_2^-, and CrO_2^- ions and increasing intensity of Al_2^-, $AlOF^-$ ions, and
- the last one from 310 s of sputtering time characterized by a stable Al_2^- ions intensity, which is defined as the substrate region. The other ions such as Cu^-, MgO^- are also representative of the AA substrate composition.

The Cu^- ion signal is nearly constant over the sputtering time corresponding to the TCP conversion

layer, then exhibits a bump in the interfacial region, and finally displays a stable intensity in the substrate region. A characteristic high intensity of ions depth profiles in the interfacial region can be also observed for MgO^-, $AlOF^-$, AlO_2^- and less significant for $^{18}O^-$ ion signal. The maximum signal observed for these ions in the interfacial region/inner TCP region can originate from a matrix effect and thus a different sputtering yield in comparison with TCP matrices as observed previously [30, 34]. It should be noted that the enrichment of certain compounds, particularly copper at the TCP/aluminium substrate interfacial region was also widely discussed in the literature [35-39]. The interfacial copper enrichment was evidenced by XPS depth profiles [35] and by TEM analysis [36] for the aluminium alloy substrates, which experienced the deoxidation process prior the TCP deposition. The presence of copper in the interfacial region was explained by the preferential dissolution of aluminium and enrichment of the other alloy elements particularly copper as demonstrated by Harvey *et al*. [40]. The quantity of copper enrichment can depend on the conditions of deoxidation (type of deoxidation solution, time and temperature of deoxidation) [40]. Higher temperature and longer time of deoxidation can lead to more important enrichment in copper but also to more significant morphological surface modifications with formation of scalloped structure [40]. It should be noted that the copper enrichment can be detrimental to the corrosion behavior of aluminium alloys coated by conversion coatings as evidenced in the case of CCC coated alloys [41,42] and most recently in case of TCP coating [43]. The other compounds such as aluminium oxides, fluorooxides and magnesium oxides, represented by AlO_2^-, $AlOF^-$ ions, respectively, show similarly as for the Cu^- signal, an increased intensity in the inner part /interfacial zone. These results confirm a bi-layered structure of TCP coating as shown in Figure 2 (a) with the outer (rich in zirconium and chromium) and inner part (aluminium oxide, and oxyfluorure of aluminium and copper) [26,44-49]. The MgO^- ion signal shows a peaked intensity in the outer part of TCP layer just during the first few seconds of sputtering, then the signal is almost completely attenuated, then increases and stabilizes in the interfacial, substrate region, respectively. According to our knowledge the enrichment of the inner TCP layer in magnesium oxide was rarely discussed

in the literature [49]. It should be emphasized here that the ToF-SIMS ion depth profiles for TCP coating with 5 minutes of PACS post-treatment presented in Figure 1 (b) are almost identical to the TCP coating without post-treatment (Figure 1(a)). Thus, it can be concluded that the PACS post-treatment for 5 minutes does not affect the TCP coating composition or its bi-layered structure. Figure 2 (a) and (b) present the structure and composition of the TCP conversion layer without and with PACS post-treatment, respectively.

The total thickness of the conversion layer with and without post-treatment was determined by coupling, ToF-SIMS negative ion in-depth profiles with profilometry measurements of the crater depth. To do so, the conversion layer was sputtered to attain the substrate (around 310 s of sputtering as indicated in Figure 1 a and b. The mean value of the sputtering rate was 0.29 nm/s (± 0.02 nm/s). The thicknesses of the conversion layers with and without post-treatment (presented in Figure 1 (a) and (b) are the same: 90 nm (310 ± 10 s of sputtering) and 91 nm (315 s ± 10 s of sputtering), respectively.

To be able to determine the distribution of lanthanum in the conversion layer after PACS post-treatment the ToF-SIMS positive ion depth profiles were performed for the same sample (Figure 1 (c). At the same time La^+ signal and the other positive ions such as Cr^+, Zr^+, Al^+, Mg^+, Mn^+ and Fe^+ were recorded. The Cr^+, Zr^+, La^+ ions are representative of the TCP coating composition with the PACS post-treatment containing the La inhibitor as indicated in the experimental part and the other ions are representative of the AA 2024 substrate. Similarly, to the negative ion depth profiles, the positive ion profiles present similar bi-layered coating structure with the outer TCP and inner TCP layer (interface region). The La^+ ion intensity signal is the most intense in outer part, and rapidly declines when reaching the inner part of the TCP layer. It can be then concluded that the distribution of lanthanum is not homogenous in depth. These results are in agreement with our previous studies [25].

Figure 3 presents the influence of PACS time post-treatment (5, 10 and 30 minutes) on the distribution of La (Figure 3 (a) and on the ratio of Cr^-/Zr^- ion signals (Figure 3 (b)). As the time of

PACS post-treatment increases the La^+ ion signal intensity increases also from approximately 70 to 200 counts. Slightly different La profile can be observed for the TCP sample with 10 minutes of post-treatment. In this case, the maximum intensity of La signal is shifted to higher sputtering time (180 s) indicating that the coating can be locally thicker or showing a non-homogenous distribution of La-containing species inlayed into the TCP coating. The Cr^-/Zr^- ratio shows a decrease as a function of PACS post-treatment time. However, this decrease is less obvious for 30 minutes of post-treatment, which can be influenced by local coating heterogeneities.

The distribution of La species over the aluminium alloy matrix and intermetallic particles was also investigated by 3-dimensional (3D) ToF-SIMS imaging performed in the positive ions mode (Fig. 4). The principle of 3D ToF-SIMS technique is to record the 2D chemical images at different sputtering depths, which then are reconstructed to report the three-dimensional images of TCP post-treated coating elucidating spatial and chemical heterogeneity.

La^+ and LaO^+ signals observed in Fig. 4 show the same intensity over the Cu-rich intermetallic particles (Al_6(Cu, Fe, Mn) and aluminium matrix indicating their homogenous surface distribution. The Cr and Zr-species show slight enrichment over the Cu-rich IMP. Based on the ToF-SIMS images (Fig. 4) and also ToF-SIMS depth profiles presented above (Fig. 1 and 3), it can be then concluded that the La-species essentially present in the outer part of the TCP layer, are homogenously distributed. It should be emphasized that despite slight local heterogeneities of Zr and Cr, the uniform distribution of La-species can play an important inhibitor role in filling the coating defects and/or pores and at the same time increasing the barrier properties of the TCP coating.

In order to confirm the TCP coating structure, its composition and the distribution of the La species as a function of PACS post-treatment the GD-OES elemental depth profiles were performed. The area of GD-OES analysis is 4 mm of diameter, so the measurements are averaged over a large area compared to ToF-SIMS (100 x 100 μm^2). It should be also noted, that the coated samples submitted

to the ultra-high vacuum during ToF-SIMS measurements can also suffer more important coating dehydration and formation of defects (cracking and exfoliation) [50,51] contrary to the short exposition (~10 minutes) to the law vacuum (lower than ~10^{-2} mbar) during the GD-OES measurements. As presented in Figure 5 (a), GD-OES elemental profiles confirm the bi-layered (outer and inner (interfacial)) coating structure observed already by ToF-SIMS. The post-treatment time does not influence the thickness of the TCP coating, however, changes in the Cr distribution and concentration are observed. Cr signal shows a clear intensity decrease and more homogenous distribution in the outer part of the TCP layer. Figure 5 (b) shows also a decrease of the Cr/Zr ratio, whereas the La signal shows an increases with the increase of post-treatment time (Figure 5 (c)). The increase of La observed by GD-OES in the outer part of the TCP layer is in agreement with the ToF-SIMS analysis.

XPS analysis was performed to evaluate the surface composition of the TCP coating before and after post-treatment (5 and 30 minutes). Figure 6 presents the Al 2p and Cu 2p core level signals corresponding to the AA 2024 substrate, and Cr 2p, Zr 3d and La 3d corresponding to the TCP composition without and with PACS post-treatment. The XPS analysis of TCP coating without PACS post-treatment shows clearly the presence of Al and Cu signals (Figure 6 a, b, respectively), which correspond to the AA 2024 substrate meaning that the coating is thin, non-homogenous and/or present some defects as already observed previously [52]. The coverage factor by the TCP coating can be also influenced by the surface state and the surface pre-treatments of the AA 2024 substrate as also discussed previously [52]. After PACS post-treatment (5 or 30 minutes) the Al and Cu signals are no longer observed, which suggests improved coating thickness and/or its quality (the coating more homogenous, less porous and/or defective). A formation of better quality coating with less defects or cracks was already observed by SEM characterization in our previous work [25]. Cr and Zr signals can be observed on the TCP coating after 0, 5 and 30 minutes of the PACS post-treatment. The XPS analysis of TCP coating was presented in details in our previous works [25,52]. The Cr 2p spectrum shows a spin orbit doublet with two peaks Cr $2p_{3/2}$ and Cr $2p_{1/2}$ but due to clear

separation of these two Cr 2p peaks (9.8 eV), only the Cr $2p_{3/2}$ is presented here (Figure 6 (c)). As discussed previously the decomposition of Cr 2p is quite complex [25,52] and three components assigned to chromium oxides, hydroxides and fluorides/oxyfluorides can be present on the TCP surface without post-treatment [25,52]. A broad Cr 2p peak at around 577 eV can be attributed to Cr_2O_3 and to $Cr(OH)_3$ [49,53-58]. Already after 5 minutes of PACS post-treatment a higher binding energy peak at around 579 eV corresponding to chromate species (Cr(VI) oxide or hydroxides) can be observed [53,57-59]. With the increase of the post-treatment time the intensity of this peak increases slightly. The presence of the Cr(VI) was also clearly observed in our previous studies where the same PACS post-treatment was applied [25]. However, it should be emphasized that it was demonstrated that the Cr(VI) was detected only on the extreme surface and not inside the TCP conversion layer. Despite the thicker conversion layer and the presence of higher Cr $2p_{3/2}$ peak corresponding to Cr (VI), the total concentration of Cr(VI) in the post-treated TCP layer was estimated to be below 0.1 wt% [25]. Thus, as mentioned in the introduction, this low quantity of Cr(VI) is much lower than the quantity authorized by REACh regulations [9] and it should not hinder the future application of the PACS post-treatment.

The Zr 3d spectrum (Figure 6 (d)) shows a Zr $3d_{5/2}$ and $3d_{3/2}$ spin-orbit doublet at binding energies of 182 and 185 eV, respectively, corresponding to the zirconium oxide ZrO_2 in agreement with previous studies [52,60,61]. No chemical modification of Zr 3d signal induced by post-treatment but only a small intensity increase for 30 minutes of post-treatment is observed.

The La signal was clearly observed after 5 and 30 minutes of PACS post-treatment (Figure 6 (e)). The spectra present characteristic spin orbit doublet of La $3d_{5/2}$ and La $3d_{3/2}$, however here for simplicity only La $3d_{5/2}$ is present. Different peaks can be distinguished here: the low binding energy peak at around 830 eV corresponding to the Auger KLL of fluorine [53], and the higher binding energy peaks at around 835 eV corresponding to $La(OH)_3$ [25,62,63], the peak at around 839 eV to LaF_3 and finally the shake-up satellite peak at 843 eV. After 30 minutes of PACS post-treatment time, the small increase of relative intensity of lanthanum fluorides to lanthanum

hydroxides/oxides can be observed. The increase of fluorides species in place of oxides (and/or hydroxides) in the post-treated TCP layer can lead to lower corrosion resistance as evidenced previously [22,25]. Thus, it can be concluded that there is a limited time of post-treatment leading to optimal coating composition with La enrichment, most particularly in the lanthanum oxide and/or hydroxides state. The important role is also the optimization of Cr/Zr ratio in the outer part of the TCP layer, which varies as a function of PACS post-treatment time as evidenced by the ToF-SIMS and GD-OES results. The optimal post-treatment time can be determined by combining the surface characterization with electrochemical studies presented hereafter.

3.2 *In situ* OCP control during the TCP and PACS post-treatment

In order to better understand the differences between the mechanism of formation of TCP conversion layer and the PACS post-treatment, the open circuit potential (OCP) was recorded (*in situ*) during the sample immersion in the respective baths (Figure 7). It should be noted that the final potential of TCP formation is much lower (-0.92 V *vs* SCE) then the final potential of post-treatment process (-0.04 *vs* SCE). However, the shape of OCP curves are very similar for both processes and shows three characteristic regions: a rapid decrease in the first few seconds then a slight potential increase and a potential stabilization. These three principal stages correspond to the attack of the existing oxide layer (alumina or conversion layer in the case of TCP or PACS post-treatment processes, respectively) and then to the grow of the corresponding layer. A similar shape of OCP during the TCP formation was already reported by different authors [26,44,46]. The first stage of potential decrease corresponds to the attack of the alumina layer by the fluoride ions present in the TCP bath [26]. The mechanism of TCP formation in three consecutive stages was explained by the formation of bi-layered TCP structure. The formation of the inner layer is initiated by the fast pH increase at the alloy interface and then the formation of outer dense layer by the formation of $Cr(OH)_x^{(3-x)+}$ and $Zr(OH)_x^{(4-x)+}$ cations, which diffuse and hydrolyse at the cathodic sites of metal/alloy surface. Reduction of protons occurs locally at the cathodic sites and leads to precipitation of zirconium and chromium. Once the first convertion layer is formed, the process of

protons reduction is displaced to new cathodic site where the precipitation can occur. It should be noted that this localised precipitation can be a reason of formation of hetereogenous TCP layer contaning some defects as mentioned above [45]. Contrary to the *in situ* OCP measurements during the TCP formation, the *in situ* control of potential evolution during the post-treatment process was not reported in the literature. In the case of post-treatment process, the first OCP region showing a rapid potential decrease corresponds to the attact of TCP conversion layer principally by the H_2O_2 present in the PACS post-treatment bath. As a strong oxidiser, H_2O_2, if used solely in a post-treatment process, can lead to oxidation of Cr^{3+} to Cr^{6+} as reported previously[64]. However, according to Pourbaix diagrams [65], the potential of post-treatment is too low to have the oxidation of Cr^{3+} to Cr^{6+} and the zirconium oxide is stable in this range of potentials and pH (+0.2 V *vs* SHE and $4.0 < pH < 5.0$). However, the chromium oxidation with formation of Cr^{6+} during the first seconds of post-treatment can not be completely excluded due to possible local pH surface increase. It should be emphasized that this process leads only to slight surface modifications of the TCP layer as previosuly evidenced by XPS depth profiling [25]. The TCP modifications in the first seconds of immersion in post-treatment bath are necessary and allow for diffussion of La into the defects and pores of the TCP layer. As a consequence, the outer part of the TCP layer is enriched in La ions as evidenced by GD-OES and ToF-SIMS depth profiles. The TCP modifications with a small dissolution of conversion layer, particulary impoverishment in Cr-compounds (Cr/Zr ratio decrease) was also confirmed by ToF-SIMS and GD-OES results presented above. As it can be seen during the post-treatment process (1800 s, Figure 7), the potential is not stable after 600 s and continues slightly to increase to 1000 s. The gradual potential increase would suggest the progressive uptake of La-compounds. It can be expected that the TCP post-treated coating does not change significantly after post-treatment longer than 1000 s. A stabilization of OCP can indicate a reaching the optimal properties of post-treated conversion coating, which can be related to the thickening of the post-treated TCP layer and/or sealing of coating defects and pores. The coating thickening can be excluded based on the ToF-SIMS and GD-OES depth profiles results presented above. The

reaching of constant potential can be explained by the sealing of coating defects and pores, which leads to the lower ionic and electronic conductivity of the coating where the reduction of La species and oxidation of Al and/or partial dissolution of TCP coating compounds can occur. Similar mechanism was shown for the formation of chromate conversion coatings [66,67].

The electrochemical behavior of TCP coated AA 2024–T3 as a function of post-treatment time will be presented hereafter to confirm the hypothesis of optimal properties of post-treated TCP coating.

3.3 Influence of PACS post-treatment time on electrochemical behavior

Figure 8a and b show the linear sweep voltammetry (LSV) and electrochemical impedance spectroscopy (EIS) curves, respectively, recorded in 10^{-3} M NaCl + 10^{-1} M Na_2SO_4 (pH ~ 7) electrolyte for the bare AA 2024 samples and the samples with TCP coating without and with PACS time post-treatments, for times ranging from 2 to 30 minutes.

The LSV curves (Figure 8 (a)) were performed with a scan rate of 2 mV s^{-1} between -1.2 V *vs* SCE and 0.6 V *vs* SCE. All curves show the cathodic and anodic branches. According to the thermodynamics of oxidation-reduction reactions in this range of potentials, the cathodic process between ~ -0.8 V and ~ - 0.65 V corresponds to the dissolved oxygen reduction. The anodic process corresponds to the dissolution of Al alloys and S-phase (Al_2CuMg) [68]. During the anodic process for the bare AA 2024 sample and the samples without PACS post-treatment or with short PACS post-treatment immersion time (2 minutes) anodic peaks between 0.1 and 0.3 V are observed ("A" peaks). These peaks correspond to the oxidation of Cu to Cu^+ and Cu^{2+} present in Cu-rich intermetallic particles [8,17]. For the longer times of PACS post-treatment (from 5 minutes of PACS post-treatment) these peaks are not observed indicating a good sealing properties of the TCP provided by the PACS post-treatment process. These results are in agreement with the XPS and ToF-SIMS 3D imaging presented above, where no Cu can be observed on the surface of TCP with

PACS post-treatment. The anodic current below 0 V (potential lower that the potentials of "A" peaks) shows a slight increase with the increasing of PACS time post-treatment. This effect may be explained by the reduction of Cr content in the TCP outer layer due to PACS treatment as showed by GD-OES profiles in Figure 5, which seems to reduce its barrier effect against the dissolution of the Al alloy substrate.

By increasing the PACS post-treatment time a decrease of the current exchange calculated from Tafel slopes and the cathodic current can be observed. For TCP without PACS post-treatment and with 30 min of PACS post-treatment a decrease of one order of magnitude of current exchange from 3.2 10^{-3} to 1.8 10^{-4} μA cm^{-2} can be observed. This behaviour can be explained by the beneficial effect of lanthanum, which is responsible for inhibition of cathodic processes. As reported in the literature, the salts of rare earth metals can provide the corrosion inhibition for aluminium alloys [69-71]. Lanthanum present in the PACS post-treatment solution control the cathodic reaction by precipitating metal oxide (La_2O_3) and hydroxide ($La(OH)_3$) locally where the increase of pH occurs due to oxygen reduction [68,71-73]. The presence of ($La(OH)_3$) was also evidenced by XPS. The principal presence of $La(OH)_3$ and not La_2O_3 can be explained by a very hygroscopic character of La_2O_3 [74, 75] as discussed in our previous work [25].

To confirm the improved electrochemical properties of the TCP coating post-treated by PACS, EIS measurements were performed on the bare AA 2024 and TCP samples without and with PACS post-treatment (Figure 8 b, c and Table 1). The Nyquist plots obtained from the EIS measurements presented in Figure 8 (b)) demonstrate the increase of the diameter of the depressed semicircle corresponding to the overall impedance with the PACS post-treatment time. The clear increase of the overall impedance can be also observed for the sample with TCP coating with reference to the bare AA 2024 sample indicating the improved corrosion properties delivered by the TCP coating. In order to obtain additional information, the EIS spectra were modelled according to the equivalent circuit shown in Figure 8 (c)) and the parameters of fitting are depicted in Table 1. R_{el} is the electrolyte resistance, R_{coat} is the coating resistance and Q_{coat} represents a non-ideal coating

capacitance (responsible of the depleted semicircle), which is in this case a constant phase element with an impedance $Z = (j\omega)^{-n}Q^{-1}$. The parameter n is associated with the coating heterogeneity or inhomogeneous surface properties as already widely discussed in literature [76-79]. R_p is the polarisation resistance corresponding to the charge transfer of both anodic and cathodic processes present at the open circuit potential at which the EIS measurements were performed and Q_{dl} is the electrolyte-metal interfacial capacitance in the coating's pores. A similar equivalent circuit with two time constants was used previously for fitting the EIS spectra obtained for the conversion coatings based on Cr^{3+} deposited on AA 2024 [17,44]. As reported in Table 1, R_p increases until 30 minutes of post-treatment time, which can be explained by the reduced activity at the substrate/coating interface provided by the presence of lanthanum. The inhibition action of lanthanum is related to reduced oxygen reduction, which leads to the increase of the polarisation resistance. The most significant effect on the increase of R_p can be observed up to 10 minutes of PACS post-treatment time (Table 1). For longer time of post-treatment, the effect of the PACS is less significant. It can be then concluded that there is an optimal time of post-treatment responsible for the best electrochemical properties, which is related on the uptake of La ions and limited impoverishment of TCP layer compounds, particularly the chromium compounds as observed by GD-OES and ToF-SIMS depth profiles. The increase of R_{coat} with the PACS post-treatment time is observed (Table 1). The increase of R_{coat} value means that the PACS post-treatment has an effect on the coating conductivity and the increase of the coating sealing properties. These results are in good agreement with our previous data obtained on TCP coating after post-treatment showing a lower coating porosity and/or decreased number of defects and cracks [25]. The values of Q_{coat} are in good agreement with the values usually reported in literature for TCP coatings [44]; also the n_{coat} values close to 0.9 are in good agreement and are related to the local coating heterogeneities. The formation of hetereogenous TCP layer with some defects was already confirmed by SEM characterisation [25, 45]. Here, the ToF-SIMS depth profiles and and the 3D ToF-SIMS imaging

confirm the formation of the hetergenous coating especially in terms of the spatial and chemical distribution of Cr and Zr species.

4. Conclusions

1. The post-treatment does not influence the thickness and the bi-layered structure of the TCP coating as evidenced by both analytical methods ToF-SIMS and GD-OES depth profiles.

2. 3D ToF-SIMS images provide direct evidence of slight enrichment of Cr and Zr-species over the surface of Cu-rich intermetallic particles with reference to the aluminium alloy matrix.

3. La-species in the near-surface of the coating after post-treatment show a homogenous distribution as evidenced by 3D ToF-SIM, which play an important role in sealing coating defects and increasing the barrier properties of the TCP coating. The La content is higher in the outer part of the TCP coating and its concentration increases with increasing post-treatment time as revealed by both ToF-SIMS and GD-OES depth profiles.

4. XPS results reveal a limited time of post-treatment leading to optimal coating composition enriched in La, most particularly in the lanthanum oxide and/or hydroxides.

5. A significant inhibition of the cathodic oxygen reduction is obtained with increasing of post-treatment time.

6. Increasing the post-treatment time may lead to a lower content of Cr-species on the coating surface, which can affect the anodic protection as observed by the electrochemical measurements.

7. The electrochemical measurements (OCP, LSV and EIS) show that the optimal post-

treatment time of TCP coating is 10 minutes, which corresponds to sufficient enrichment in the La compounds and not significant impoverishment in Cr species in the outer part of the TCP coating.

Acknowledgements:

Financial support by DGA-France, the Région Occitanie/Pyrénées-Méditerranée and the EU (FEDER/ERDF) in the frame of NEPAL FUI project is acknowledged.

References

[1] E. A. Starke, J. T. Staley, Application of modern aluminum alloys to aircraft, Prog. Aerospace Sci. 32 (1996) 131-172. https://doi.org/10.1016/0376-0421(95)00004-6.

[2] G. Valérie, G. Mankowski, Localized corrosion of 2024 T351 aluminium alloy in chloride media, Corros. Sci. 41 (1998) 421-438. https://doi.org/10.1016/S0010-938X(98)00116-4.

[3] Z. Liu, P. H. Chong, A. N. Butt, P. Skeldon, G. E. Thompson, Corrosion mechanism of laser-melted AA 2014 and AA 2024 alloys, Appl. Surf. Sci. 247 (2005) 294-299. https://doi.org/10.1016/j.apsusc.2005.01.067.

[4] I. T. E. Fonseca, N. Lima, J. A. Rodrigues, M. I. S. Pereira, J. C. S.Salvador, M. G. S. Ferreira, Passivity breakdown of Al 2024-T3 alloy in chloride solutions: a test of the point defect model, Electrochem. Commun. 4 (2002) 353-357.

[5] R.G. Buchheit, L.P. Montes, M.A. Martinez, J. Michael, P.F. Hlava, The Electrochemical Characteristics of Bulk- Synthesized Al2CuMg, J. Electrochem. Soc., 146 (1999) 4424-4428. https://doi.org/10.1149/1.1392654.

[6] R.G. Buchheit, M.A. Martinez, L.P. Montes, Evidence for Cu Ion Formation by Dissolution and Dealloying the Al2CuMg Intermetallic Compound in Rotating Ring- Disk Collection Experiments, J. Electrochem. Soc., 147 (2000) 119-124. https://doi.org/10.1149/1.1393164.

[7] M. L. Zheludkevich, K. A. Yasakau, S. K. Poznyak, M. G. S. Ferreira, Triazole and thiazole derivatives as corrosion inhibitors for AA2024 aluminium alloy, Corros. Sci. 47 (2005) 3368- 3383. https://doi.org/0.1016/j.corsci.2005.05.040.

[8] J. Qi, A. Němcová, J. R.Walton, X. Zhoua, P. Skeldon, G. E. Thompson, Influence of pre- and post-treatments on formation of a trivalent chromium conversion coating on AA2024 alloy, Thin Solid Films, 616 (2016) 270-278. https://doi.org/10.1016/j.tsf.2016.08.044.

[9] European Chemical Agency, REACh Annex XIV.

[10] Occupational Exposure to Hexavalent Chromium, US Dept. of Labor, OSHA Federal Register # 71:10099-10385, 28 Feb2006.

[11] G. O. Ilevbare, O. Schneider, R. G. Kelly, and J. R. Scully, In Situ Confocal Laser Scanning Microscopy of AA 2024-T3 Corrosion Metrology I. Localized Corrosion of Particles, J. Electrochem. Soc., 151 (2004) B453-B464. https://doi.org/10.1149/1.1764780.

[12] N. Birbilis and R. G. Buchheit, Electrochemical Characteristics of Intermetallic Phases in Aluminum Alloys An Experimental Survey and Discussion, J. Electrochem. Soc., 152 (2005) B140-B151. https://doi.org/10.1149/1.1869984.

[13] N. Birbilis and R. G. Buchheit, Investigation and Discussion of Characteristics for Intermetallic Phases Common to Aluminum Alloys as a Function of Solution pH, J. Electrochem. Soc., 155 (2008) C117-C126. https://doi.org/10.1149/1.2829897.

[14] Occupational Exposure to Hexavalent Chromium, United States Department of Labor, US, 2006.

[15] M.W. Kendig, R.G. Buchheit, Corrosion inhibition of aluminum and aluminum alloys by

soluble chromates, chromate coatings, and chromate-free coatings, Corrosion 59 (2003) 379–400. https://doi.org/10.5006/1.3277570.

[16] F. Pearistein, V.S. Agarwala, Trivalent chromium solutions for applying chemical conversion coatings to aluminium alloys or for sealing anodised aluminium, Plat. Surf. Finish. 81 (1994) 50–55. https://doi.org/

[17] L. Li, A.L. Desouza, and G. M. Swaina, Effect of Deoxidation Pretreatment on the Corrosion Inhibition Provided by a Trivalent Chromium Process (TCP) Conversion Coating on AA2024-T3, J. Electrochem. Soc., 161 (5) (2014) C246-C253. https://doi.org/10.1149/2.031405jes.

[18] Y. Guo, G.S. Frankel, Active corrosion inhibition of AA 2024-T3 by trivalent chrome process treatment, Corrosion 68 (2012) 1–10. https://doi.org/10.5006/0010-9312-68-4-3.

[19] C.A. Matzdorf, W.C. Nickerson, E. Lipnickas, Evaluation of modified zirconium/trivalent chromium conversion coatings by accelerated corrosion and electrochemical techniques, Proc. 2005 Tri-Service Corrosion Conference, Orlando, Florida, U.S.A., 2005.

[20] T. Schram, G. Goeminne, H. Terryn, W. Vanhoolst, P. Van Espen, Study of the Composition of Zirconium based Chromium free Conversion Layers on Aluminium, Trans. Inst. Met. Finish. 73 (1995) 91-97. https://doi.org/10.1080/00202967.1995.11871066.

[21] X. Zhang, C. Van den Bos, W. G. Sloof, A. Hovestad, H.Terryn, J. H. W. de Wit, Comparison of the morphology and corrosion performance of Cr(VI)- and Cr(III)-based conversion coatings on zinc, Surf. Coat. Technol. 199 (2005) 92-104. https://doi.org/10.1016/j.surfcoat.2004.12.002.

[22] J. Qi, T. Hashimoto, G. E. Thompson, and J. Carr, Influence of Water Immersion Post-Treatment Parameters on Trivalent Chromium Conversion Coatings Formed on AA2024-T351 Alloy, J. Electrochem. Soc., 163 (2016) 131-138. https://doi.org/10.1149/2.0221605jes.

[23] H. Zhang and Y. Zuo, The improvement of corrosion resistance of Ce conversion films on aluminum alloy by phosphate post-treatment, Appl. Surf. Sci., 254 (2008) 4930-4935. https://doi.org/10.1016/j.apsusc.2007.12.066.

[24] D. K. Heller, W. G. Fahrenholtz, and M. J. O'Keefe, Effect of Phosphate Source on Post-Treatment of Cerium-Based Conversion Coatings on Al 2024-T3, J. Electrochem. Soc., 156, (2009) C400-C406. https://doi.org/10.1149/1.3224005.

[25] M. Ely, J. Światowska, A. Seyeux, S. Zanna, P. Marcus, Role of Post-Treatment in Improved Corrosion Behavior of Trivalent Chromium Protection (TCP) Coating Deposited on Aluminum Alloy 2024-T3, J. Electrochem. Soc. 164 (2017) C276-C284. https://doi.org/10.1149/2.0431706jes.

[26] L. Li, G. P. Swain, A. Howell, D. Woodbury & G. M. Swain, The Formation, Structure, Electrochemical Properties and Stability of Trivalent Chrome Process (TCP) Coatings on AA 2024. J. Electrochem. Soc. 158 (2011) C274–C283. https://doi.org/10.1149/1.3607980.

[27] L. L. Li, G. M. Swain, Effects of aging temperature and time on the corrosion protection provided by trivalent chromium process coatings on AA2024-T3, ACS Appl. Mater. Interface, 5 (2013) 7923-7930. https://doi.org/10.1021/am4020023.

[28] P. Bares, C. Stephan, C. Gazeau, Patent WO2013117767 (2013).

[29] I. S. Molchan, G. E. Thompson, P. Skeldon, N. Trigoulet, P. Chapon, A. Tempez, J. Malherbe, L. L. Revilla, N. Bordel, P. Belenguer, T. Nelis, A. Zahri, L. Therese, P. Guillot, M. Ganciu, J. Michler, M. Hohl, The concept of plasma cleaning in glow discharge spectrometry, J. Anal. At. Spectrom. 24 (2009) 734-741. https://doi.org/10.1039/B818343K.

[30] B. Díaz, E. Härkönen, J. Światowska, V. Maurice, A. Seyeux, P. Marcus, & M. Ritala, Low-temperature atomic layer deposition of Al2O3 thin coatings for corrosion protection of steel: surface and electrochemical analysis, Corros. Sci., 53 (2011) 2168-2175. https://doi.org/10.1016/j.corsci.2011.02.036.

[31] J.-T. Li, V. Maurice, J. Swiatowska-Mrowiecka, A. Seyeux, S. Zanna, L. Klein, S.-G. Sun, and P. Marcus, XPS, time-of-flight-SIMS and polarization modulation IRRAS study of Cr2O3 thin film materials as anode for lithium ion battery, Electrochim. Acta, 54 (2009) 3700-3707. https://doi.org/10.1016/j.electacta.2009.01.052.

[32] B. Diaz, J. Swiatowska, V. Maurice, A. Seyeux, B. Normand, E. Haerkoenen, M. Ritala, and P. Marcus, Electrochemical and time-of-flight secondary ion mass spectrometry analysis of ultra-thin metal oxide (Al2O3 and Ta2O5) coatings deposited by atomic layer deposition on stainless steel, Electrochim. Acta, 56 (2011) 10516-10523. https://doi.org/10.1016/j.electacta.2011.02.074.

[33] C. Pereira-Nabais, J. Swiatowska, A. Chagnes, F. Ozanam, A. Gohier, P. Tran-Van, C.-S. Cojocaru, M. Cassir, and P. Marcus, Interphase chemistry of Si electrodes used as anodes in Li-ion

Batteries, Appl. Surf. Sci., 266 (2013) 5-16. https://doi.org/10.1016/j.apsusc.2012.10.165.

[34] J. Qi, G. E. Thompson, Comparative studies of thin film growth on aluminium by AFM, TEM and GDOES characterization, Appl. Surf. Sci. 377 (2016) 109-120. https://doi.org/10.1016/j.apsusc.2016.03.115.

[35] J. Vander Kloet, A.W. Hassel & M. Stratmann Effect of Pretreatment on the Intermetallics in Aluminum Alloy 2024-T3, Zeitschrift für Phys. Chemie 219 (2005) 1505–1518. https://doi.org/10.1524/zpch.2005.219.11.1505.

[36] Y. Liu, M. A. Arenas, A. de Frutos , J. de Damborenea, A. Conde, P. Skeldon, G. E. Thompson, P. Bailey & T. C. Q. Noakes, Influence of nitric acid pre-treatment on Al–Cu alloys. Electrochim. Acta 53 (2008) 4454–4460. https://doi.org/10.1016/j.electacta.2008.01.026.

[37] C. E. Moffitt, D. M. Wieliczka & H. K. Yasuda, An XPS study of the elemental enrichment on aluminum alloy surfaces from chemical cleaning. Surf. Coatings Technol. 137 (2001) 188–196. https://doi.org/10.1016/S0257-8972(00)01121-X.

[38] Y. Liu, F. Colin, P. Skeldon, G. E. Thompson, X. Zhou, H. Habazaki & K. Shimizu, Enrichment factors for copper in aluminium alloys following chemical and electrochemical surface treatments. Corros. Sci. 45 (2003) 1539–1544. https://doi.org/10.1016/S0010-938X(02)00249-4.

[39] H. H. Strehblow, C. M. Melliar-Smith & W. M. Augustyniak, Examination of Aluminum-Copper Films during the Galvanostatic Formation of Anodic Oxide. J. Electrochem. Soc. 125 (1978) 915-919. https://doi.org/10.1149/1.2131590.

[40] T. G. Harvey, A. E. Hughes, S. G. Hardin, T. Nikpour, S. K. Toh, A. Boag, D. McCulloch & M. Horne, Non-chromate deoxidation of AA 2024-T3: Sodium bromate–nitric acid (20–60°C). Appl. Surf. Sci. 254 (2008) 3562–3575. https://doi.org/10.1016/j.apsusc.2007.11.061.

[41] X. Sun, R. Li, K. C. Wong, K. A. R. Mitchell & T. Foster, Surface effects in chromate conversion coatings on 2024-T3 aluminum alloy, J. Mater. Sci. 36 (2001) 3215–3220. https://doi.org/

[42] Q. Meng & G. S. Frankel, Effect of Copper Content on Chromate Conversion Coating Protection of 7xxx-T6 Aluminum Alloys, Corrosion 60 (2004) 897–905. https://doi.org/10.5006/1.3287823.

[43] R. Saillard, B. Viguier, G. Odemer, A. Pugliara, B. Fori and C. Blanc, Influence of the microstructure on the corrosion behaviour of 2024 aluminium alloy coated with a trivalent chromium conversion layer, Corrosion Science, 142 (2018) 119-132. https://doi.org/10.1016/j.corsci.2018.07.007.

[44] J.-T. Qi, T. Hashimoto, J. R. R. Walton, X. Zhou, P. Skeldon & G. E. E. Thompson, Trivalent chromium conversion coating formation on aluminium, Surf. Coatings Technol. 280 (2015) 317–329. https://doi.org/10.1016/j.surfcoat.2015.09.024.

[45] X. Dong, P. Wang, S. Argekar & D. W. Schaefer, Structure and composition of trivalent chromium process (TCP) films on Al alloy, Langmuir 26 (2010) 10833–10841. https://doi.org/10.1021/la100699u.

[46] W. –K. Chen, J. –L. Lee, C. –Y. Bai, K. –H. Hou & M. –D. Ger, Growth and characteristics of Cr(III)-based conversion coating on aluminum alloy, J. Taiwan Inst. Chem. Eng. 43 (2012) 989–995. https://doi.org/10.1016/j.jtice.2012.05.007.

[47] W.-K. Chen, C.-Y. Bai, C.-M. Liu, C.-S. Lin & M.-D. Ger, The effect of chromic sulfate concentration and immersion time on the structures and anticorrosive performance of the Cr(III) conversion coatings on aluminum alloys, Appl. Surf. Sci. 256 (2010) 4924–4929. https://doi.org/10.1016/j.apsusc.2010.03.003.

[48] Y. Guo & G. S. Frankel GS, Characterization of trivalent chromium process coating on AA 2024-T3, Surf. Coatings Technol. 206 (2012) 3895–3902. https://doi.org/ 10.1016/j.surfcoat. 2012.03.046 A.

[49] J. Qi, T. Hashimoto, J. Walton, X. Zhou, P. Skeldon & G.E. Thompson, Formation of a Trivalent Chromium Conversion Coating on AA 2024-T351 Alloy, J. Electrochem. Soc. 163 (2016) C25–C35. https://doi.org/10.1149/2.0771602jes.

[50] V. Laget, C. S. Jeffcoate, H. S. Isaacs & R. G. Buchheit, Dehydration-Induced Loss of Corrosion Protection Properties in Chromate Conversion Coatings on Aluminum Alloy 2024-T3, J. Electrochem. Soc. 150 (2003) B425-B432. https://doi.org/10.1149/1.1593040.

[51] T. G. Harvey, Cerium-based conversion coatings on aluminium alloys: a process review. Corros. Eng. Sci. Technol. 48 (2013) 248–269. https://doi.org/10.1179/1743278213Y.0000000089.

[52] R. Viroulaud, J. Światowska, A. Seyeux, S. Zanna, J. Tardelli, P. Marcus, Influence of Surface Pretreatments on the Quality of Trivalent Chromium Process Coatings on Aluminum Alloy, Appl. Surf. Sci. 423 (2017) 927-938. https://doi.org/10.1016/j.apsusc.2017.06.246.

[53] C. D. Wagner, W. M. Riggs, L. E. Davis, J. F. Moulder, and G. E. Muilenberg, Handbook of X-ray photoelectron spectroscopy, Perkin-Elmer Corporation Physical electronics division, (1978).

[54] M. Aronniemi, J. Sainio, and J. Lahtinen, Chemical state quantification of iron and chromium

oxides using XPS: the effect of the background subtraction method, Surf. Sci., 578 (2005) 108-123. https://doi.org/10.1016/j.susc.2005.01.019.

[55] B. Stypula and J. Stoch, The characterization of passive films on chromium electrodes by XPS, Corros. Sci., 36 (1994) 2159-2167. https://doi.org/10.1016/0010-938X(94)90014-0.

[56] W. P. Yang, D. Costa, and P. Marcus, Resistance to Pitting and Chemical Composition of Passive Films of a Fe- 17%Cr Alloy in Chloride- Containing Acid Solution, J. Electrochem. Soc., 141 (1994) 2669-2676. https://doi.org/10.1149/1.2059166.

[57] A. E. Hughes, R. J. Taylor, and B. R. W. Hinton, Chromate Conversion Coatings on 2024 Al Alloy, Surf. Interface Anal., 25 (1997) 223-234. https://doi.org/10.1002/(SICI)1096-9918(199704)25:4<223::AID-SIA225>3.0.CO;2-D.

[58] M. C. Biesinger, B. P. Payne, A. P. Grosvenor, L. W. M. Lau, A. R. Gerson, and R. S. C. Smart, Resolving surface chemical states in XPS analysis of first row transition metals, oxides and hydroxides: Cr, Mn, Fe, Co and Ni, Appl. Surf. Sci., 257 (2011) 2717-2730. https://doi.org/10.1016/j.apsusc.2010.10.051.

[59] D. Chidambaram, G. P. Halada, and C. R. Clayton, Development of a technique to prevent radiation damage of chromate conversion coatings during X-ray photoelectron spectroscopic analysis, Appl. Surf. Sci., 181 (2001) 283-295. https://doi.org/10.1016/S0169-4332(01)00433-0.

[60] A.E. Hughes, B.A. Sexton, Comments on the use of implanted Ar as a binding energy reference, J. Electron Spectrosc. Relat. Phenom. 50 (1990) C15–C18. https://doi.org/10.1016/0368-2048(90)87080-8.

[61] S. Sinha, S. Badrinarayanan, S.H. Sinha, Interaction of oxygen with Zr76Fe24 metglass: an X-ray photoelectron spectroscopy study, J. Less-Common Met. 125 (1986) 85–95. https://doi.org/10.1016/0022-5088(86)90082-2.

[62] M. F. Sunding, K. Hadidi, S. Diplas, O. M. Lovvik, T. E. Norby, and A. E. Gunnaes, XPS characterisation of in situ treated lanthanum oxide and hydroxide using tailored charge referencing and peak fitting procedures, J. Electron Spectros. Relat. Phenomena, 184 (2011) 399-409. https://doi.org/10.1016/j.elspec.2011.04.002.

[63] P. Ivanova, A. W. Naumkin, and L. A. Vasilyev, An XPS study of compositional changes induced by argon ion bombardment of the LaPO4 surface, Vacuum, 47 (1996) 67-71. https://doi.org/10.1016/0042-207X(95)00180-8.

[64] L. Li, D. Y. Kim & G. M. Swain, Transient Formation of Chromate in Trivalent Chromium Process (TCP) Coatings on AA 2024 as Probed by Raman Spectroscopy. J. Electrochem. Soc. 159 (2012) C326–C333. https://doi.org/10.1149/2.019208jes.

[65] C.T. Kwok, P.K. Wong, H.C. Man, F.T. Cheng, Effect of pH on corrosion behavior of CuCrZr in solution without and with NaCl, J. Nuclear Materials 394 (2009) 52–62. https://doi.org/10.1016/j.jnucmat.2009.08.006.

[66] P. Campestrini, G. Goeminne, H. Terryn, J. Vereecken, and J. H. W. de Wit, Chromate Conversion Coating on Aluminum Alloys I. Formation Mechanism, J. Electrochem. Soc. 151 (2004) B59-B70. https://doi.org/10.1149/1.1637355.

[67] H.A. Katzman, G.M. Malouf, R. Bauer, G.W. Stupian, Corrosion-protective chromate coatings on aluminum, Appl. Surf. Sci. 2 (1979) 416-432. https://doi.org/10.1016/0378-5963(79)90073-4.

[68] K. A. Yasakau, M. L. Zheludkevich, S. V. Lamaka, and M. G. S. Ferreira, Mechanism of Corrosion Inhibition of AA2024 by Rare-Earth Compounds, J. Phys. Chem. B, 110, (2006) 5515-5528. https://doi.org/10.1021/jp0560664.

[69] M. Bethencourt, F. J Botana, J. J. Calvino, M. Marcos, M. A. Rodriguez-Chacon, Lanthanide compounds as environmentally-friendly corrosion inhibitors of aluminium alloys: a review, Corros. Sci., 40 (1998) 1803-1819. https://doi.org/10.1016/S0010-938X(98)00077-8.

[70] R. L. Twite, G. P. Bierwagen, Review of Alternatives to Chromate for Corrosion Protection of Aluminum Aerospace Alloys, Prog. Org. Coat., 33 (1998) 91-100. https://doi.org/10.1016/S0300-9440(98)00015-0.

[71] B. Davo, J. de Damborenea, Use of rare earth salts as electrochemical corrosion inhibitors for an Al–Li–Cu (8090) alloy in 3.56% NaCl, J. Electrochim. Acta, 49 (2004) 4957-4965. https://doi.org/10.1016/j.electacta.2004.06.008.

[72] A. Aballe, M. Bethencourt, F. J. Botana, M. Marcos, CeCl3 and LaCl3 binary solutions as environment-friendly corrosion inhibitors of AA5083 Al–Mg alloy in NaCl solutions, J. Alloys Compd., 323 (2001) 855-858. https://doi.org/10.1016/j.electacta.2004.06.008.

[73] M. A. Arenas, M. Bethencourt, F. J. Botana, J. de Damborenea, M. Marcos, Inhibition of 5083 aluminium alloy and galvanised steel by lanthanide salts, Corros. Sci., 43, (2001) 157-170. https://doi.org/10.1016/S0010-938X(00)00051-2.

[74] J.-G. Kang, Y.-I. Kim, D. Won Cho, and Y. Sohn, Synthesis and physicochemical properties of La(OH)3 and La2O3 nanostructures, Mater. Sci. Semicond. Process.,40 (2015) 737-743. https://doi.org/10.1016/j.mssp.2015.07.050.

[75] P. Fleming, R. A. Farrell, J. D. Holmes, and M. A. Morris, The Rapid Formation of La(OH)3 from La2O3 Powders on Exposureto Water Vapor, J. Am. Ceram. Soc., 93 (2010) 1187-1194. https://doi.org/10.1111/j.1551-2916.2009.03564.x.

[76] L. Li, K. P. Doran, G. M. Swain, Electrochemical characterization of trivalent chromium process (TCP) coatings on aluminum alloys 6061 and 7075, J. Electrochem. Soc. 160 (2013) C396–C401. https://doi.org/10.1149/2.117308jes.

[77] J. B. Jorcin, M.E. Orazem, N. Pebere, B. Tribollet, CPE analysis by local electrochemical impedance spectroscopy, Electrochim. Acta 51 (2006) 1473–1479. https://doi.org/10.1016/j.electacta.2005.02.128.

[78] B. Díaz, E. Härkönen, V. Maurice, J. Światowska, A. Seyeux, M. Ritala, P. Marcus, Failure mechanism of thin Al2O3 coatings grown by atomic layer deposition for corrosion protection of carbon steel, Electrochim. Acta, 56, 26 (2011) 9609-9618. https://doi.org/10.1016/j.electacta.2011.07.104.

[79] B. Díaz, E. Härkönen, J. Światowska, V. Maurice, A. Seyeux, P. Marcus, M. Ritala, Low-temperature atomic layer deposition of Al2O3 thin coatings for corrosion protection of steel: surface and electrochemical analysis, Corr. Sci., 53, 6 (2011) 2168-2175. https://doi.org/10.1016/j.corsci.2011.02.036.

TABLES

Table 1. Fitting parameters of EIS spectra presented in Figure 8 (b) according to the equivalent circuit shown in Figure 8 (c).

PACS time (min)	OCP (V vs, SCE)	R_{el} ($k\Omega \cdot cm^2$)	Q_{coat} ($mS\ s^n \cdot cm^{-2}$)	n_{coat}	R_{coat} ($k\Omega \cdot cm^2$)	R_p ($k\Omega \cdot cm^2$)	Q_{dl} ($mS\ s^n \cdot cm^{-2}$)	n_{dl}	χ^2
Bare AA 2024	-0.2	0.0270 (±2.2%)	-	-	-	105 (±3.5%)	0.017000 (±2.6%)	0.87 (±0.6%)	$6.90\ 10^{-3}$
0	-0.37	0.0286 (±2.2%)	0.002025 (±18.4%)	0.85 (±2.0%)	0.3110 (±8.2%)	589 (±1.8%)	0.002945 (±12.2%)	0.92 (±1.6%)	$1.31\ 10^{-3}$
2	-0.38	0.0273± (±3.9%)	0.001942 (±25.5%)	0.83 (±2.8%)	0.4688 (±12.0%)	1385 (±4.3%)	0.003005 (±16.3%)	0.91 (±2.2%)	$3.67\ 10^{-3}$
5	-0.37	0.0270 (±3.8%)	0.001978 (±24.9%)	0.84 (±2.7%)	0.4580 (±12.1%)	1648 (±4.8%)	0.002905 (±16.8%)	0.91 (±2.3%)	$3.77\ 10^{-3}$
10	-0.49	0.0271 (±3.4%)	0.001608 (±20.7%)	0.86 (±2.2%)	0.4626 (±9.4%)	3222 (±6.0%)	0.002431 (±13.7%)	0.95 (±1.9%)	$3.51\ 10^{-3}$
30	-0.33	0.0264 (±3.2%)	0.002032 (±19.7%)	0.84 (±2.2%)	0.5086 (±10.0%)	4117 (±8.2%)	0.002931 (±13.7%)	0.91 (±1.9%)	$1.95\ 10^{-3}$

FIGURE CAPTIONS

Fig. 1 ToF-SIMS ion depth profiles: (a) and (b) negative ion depth profiles of TCP layer/ AA 2024-T3 without and with 5 minutes of PACS post-treatment, respectively; (c) positive ion depth profiles of TCP layer with 5 minutes of PACS post-treatment.

Fig. 2 Schematic representation of structure of TCP layer deposited on AA 2024-T3 substrate: (a) without post-treatment, (b) with PACS post-treatment.

Fig. 3 Influence of different times of PACS post-treatment 5, 10 and 30 minutes on: (a) ToF-SIMS positive La^+ ion depth profiles in TCP layer, (b) Cr^-/Zr^- ToF-SIMS negative ion signal ratio.

Fig. 4 3D Tof-SIMS images (100 x 100 μm^2) made in positive mode of external part of TCP layer post-treated by PACS (5 minutes).

Fig. 5 GD-OES elemental depth profiles showing the influence of post-treatment time (5, 10 and 30 minutes) on the composition of TCP layer/AA 2024: (a) Zr, Cr and Al signals, (b) Cr/Zr signal ratio, (c) La signal.

Fig. 6 Influence of PACS post-treatment time (0, 5 and 30 minutes) on the surface composition of TCP layer studied by XPS: (a) Al 2p, (b) Cu $2p_{3/2}$, (c) Cr $2p_{3/2}$, (d) Zr 3d, (e) La $3d_{5/2}$.

Fig. 7 Open circuit potentials (OCP) measurement during the TCP and PACS post-treatment for 600 s and 1800 s, respectively.

Fig. 8. (a) LSV and (b) Nyquist diagram obtained from EIS measurements (symbol - experimental points, line – fitting) recorded in 10^{-3} M NaCl + 10^{-1} M Na_2SO_4 (pH ~ 7) electrolyte for the samples with TCP coating without (TCP) and with PACS post-treatments for t=2, 5, 10 and 30 minutes; (c) the equivalent circuit used for the EIS fitting presented in figure (b).

FIGURES

Figure 1

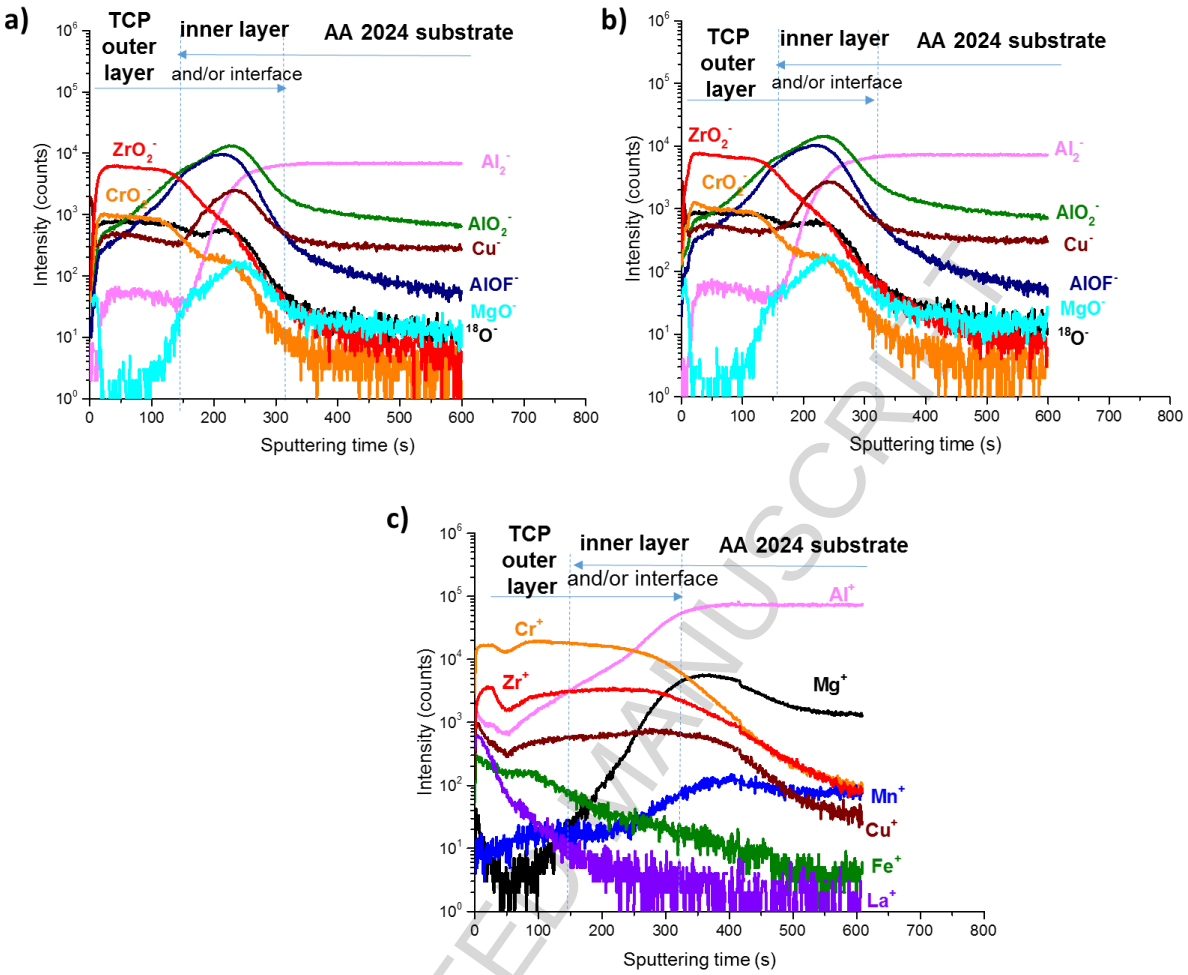

Figure 2

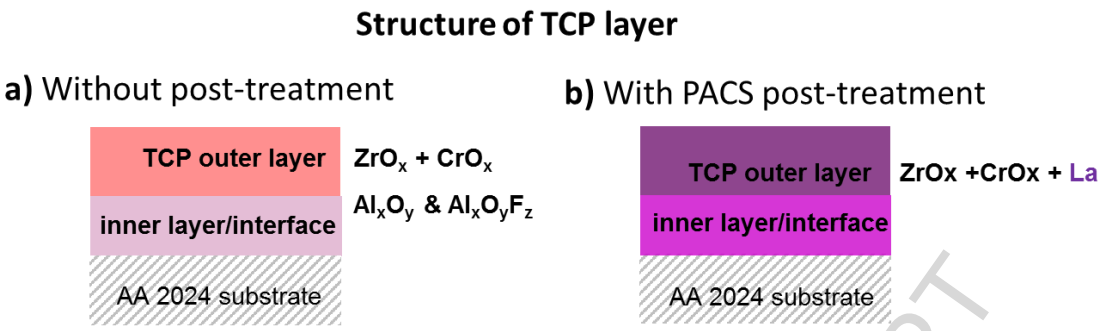

Figure 3

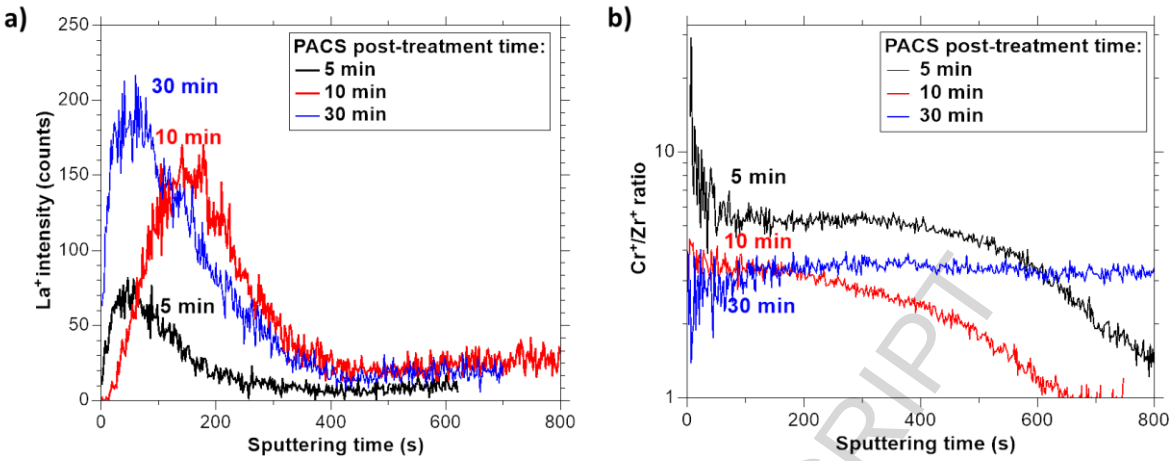

Figure 4

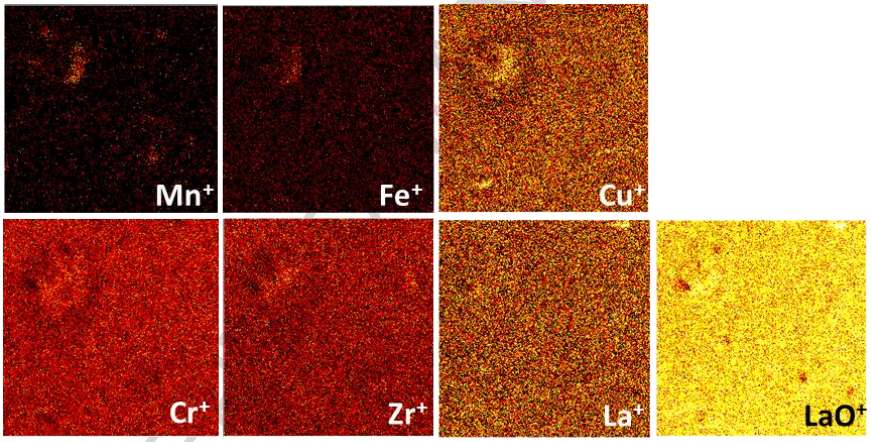

Figure 5

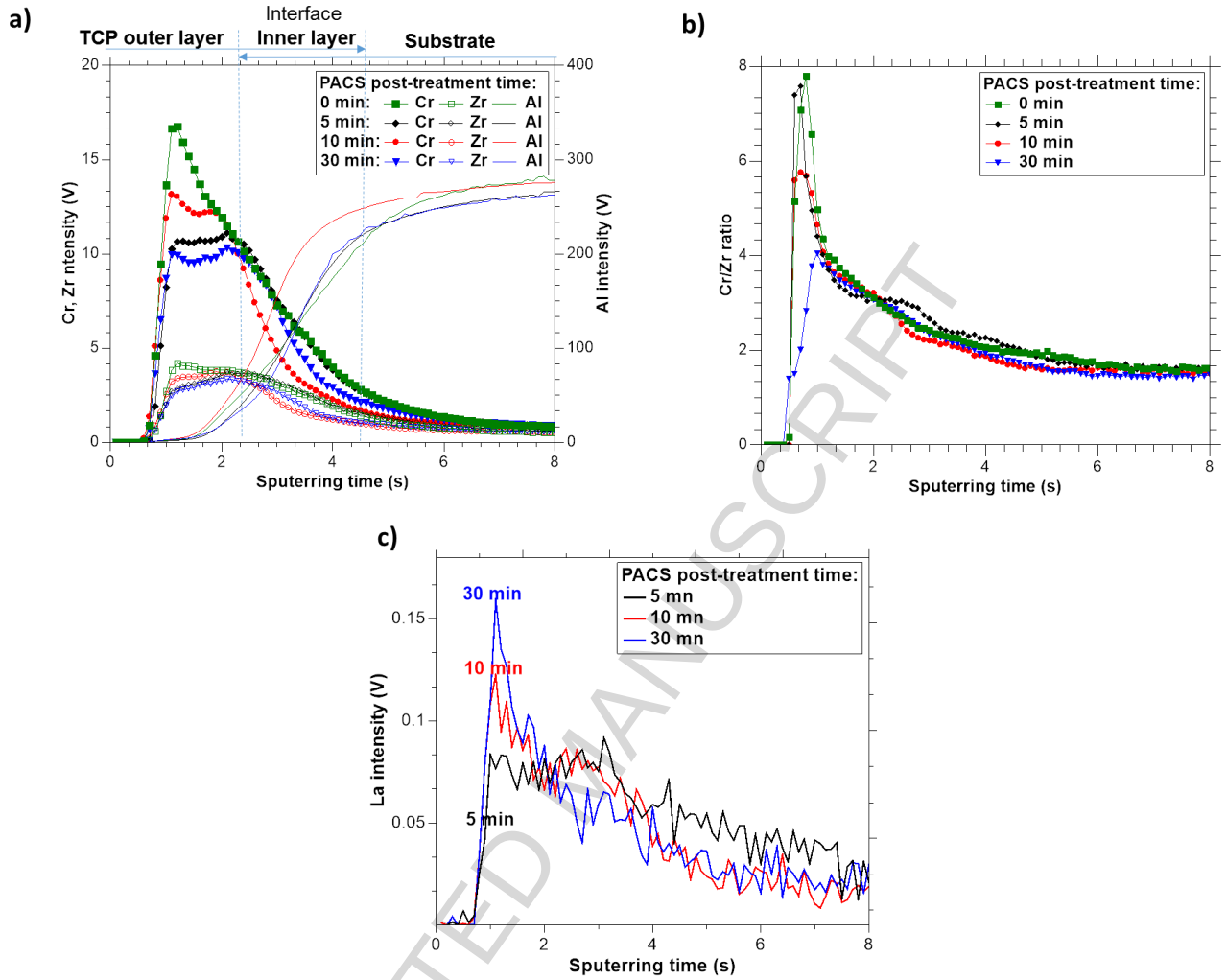

Figure 6

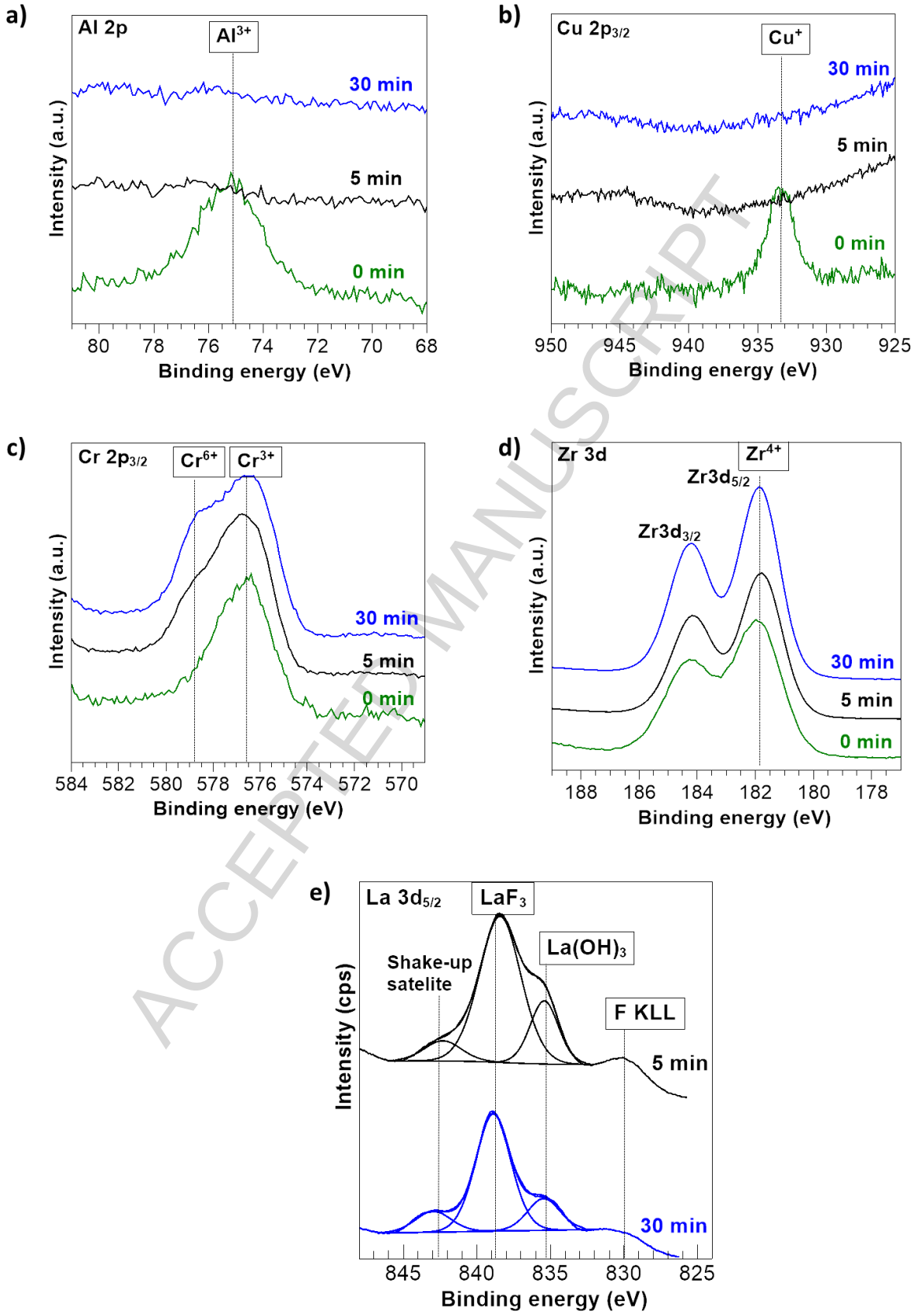

Figure 7

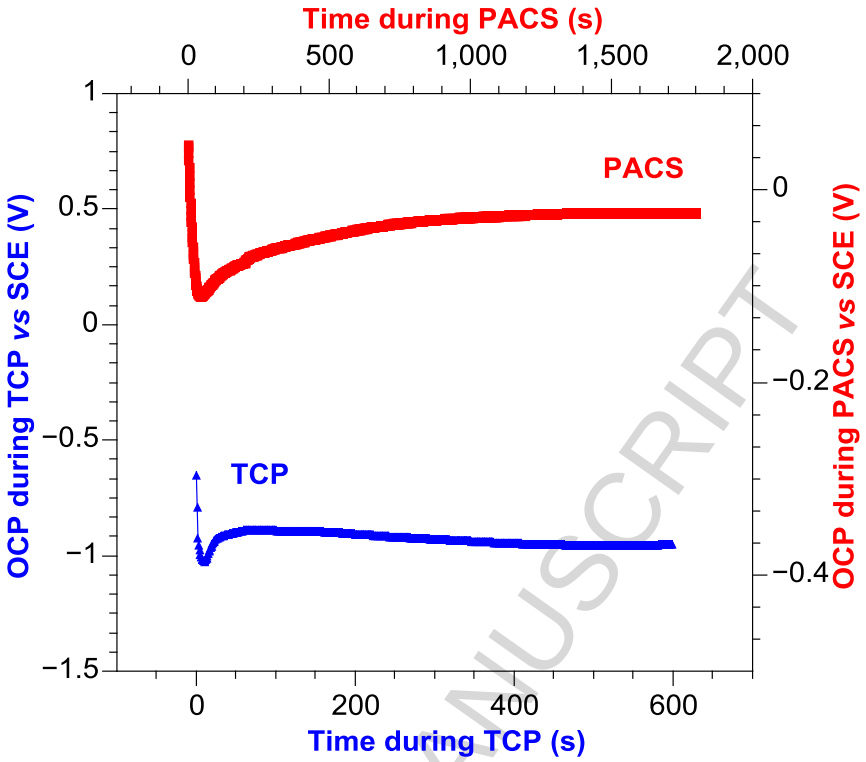

Figure 8

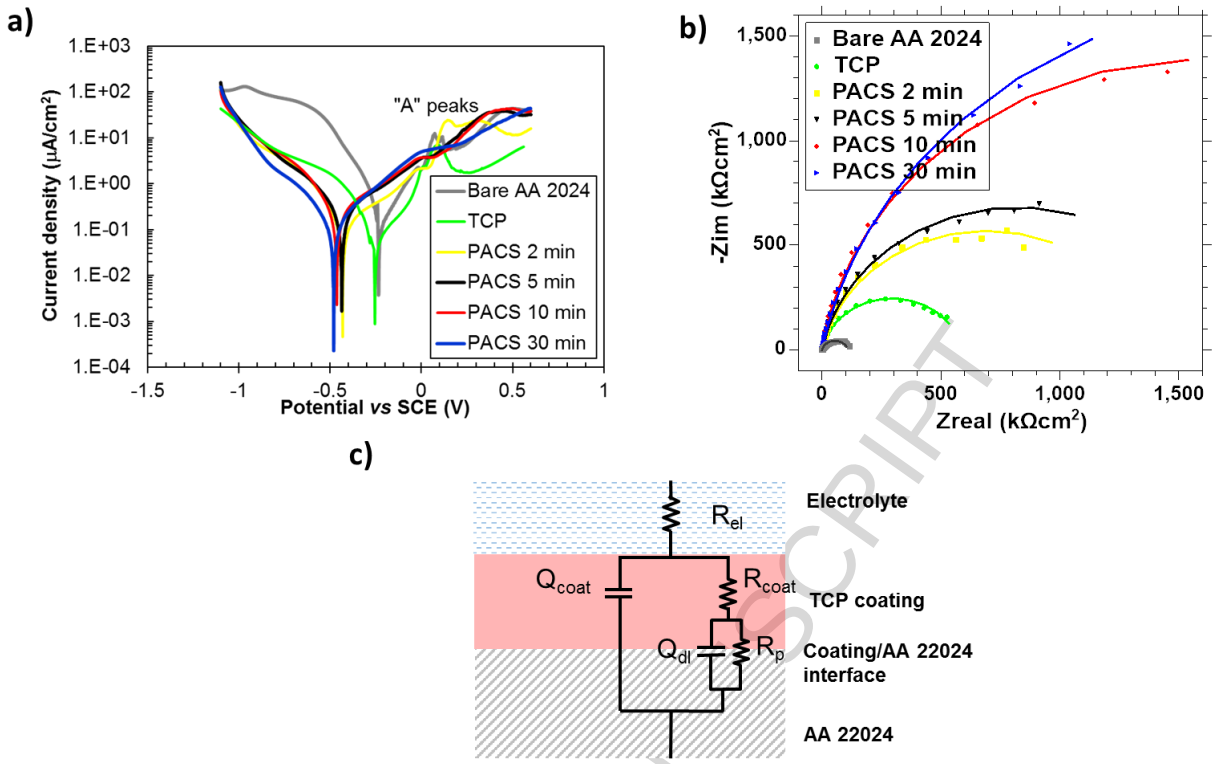

Highlights

- No thickness and structure modification of TCP coating induced by post-treatment
- Significant inhibition of the cathodic oxygen reduction induced by post-treatment
- Increase of La and decrease of Cr in TCP with higher post-treatment time
- Homogenous surface distribution of La responsible for sealing coating defects